The Pennsylvania State University
APPLIED RESEARCH LABORATORY
Post Office Box 30
State College, PA 16804

Substructure Synthesis Methods and Their Application to Structural-Acoustic Simulations

By

R. L. Campbell and C. M. Pray

Technical Report 05-012
October 2005

E. G. Liszka, Director
Applied Research Laboratory

REPORT DOCUMENTATION PAGE	Form Approved OMB No. 0704-0188

PLEASE DO NOT RETURN YOUR FORM TO THE ABOVE ADDRESS.

1. REPORT DATE *(DD-MM-YYYY)*	2. REPORT TYPE	3. DATES COVERED *(From - To)*
October 2005	Technical Report	

4. TITLE AND SUBTITLE

Substructure Synthesis Methods and Their Application to Structural-Acoustic Simulations

5a. CONTRACT NUMBER

N00024-02-D-6604

5b. GRANT NUMBER

5c. PROGRAM ELEMENT NUMBER

6. AUTHOR(S)

Robert L. Campbell and Carl M. Pray

5d. PROJECT NUMBER

5e. TASK NUMBER

5f. WORK UNIT NUMBER

7. PERFORMING ORGANIZATION NAME(S) AND ADDRESS(ES)

Applied Research Laboratory
Post Office Box 30
State College, PA 16804

8. PERFORMING ORGANIZATION REPORT NUMBER

TR 05-012

9. SPONSORING/MONITORING AGENCY NAME(S) AND ADDRESS(ES)

10. SPONSOR/MONITOR'S ACRONYM(S)

11. SPONSOR/MONITOR'S REPORT NUMBER(S)

12. DISTRIBUTION/AVAILABILITY STATEMENT

Approved for public release. Distribution unlimited

13. SUPPLEMENTARY NOTES

14. ABSTRACT

See attached.

15. SUBJECT TERMS

16. SECURITY CLASSIFICATION OF:			17. LIMITATION OF ABSTRACT	18. NUMBER OF PAGES	19a. NAME OF RESPONSIBLE PERSON
a. REPORT	b. ABSTRACT	c. THIS PAGE			19b. TELEPHONE NUMBER *(Include area code)*
Unclassified	Unclassified	Unclassified	Unclassified Unlimited-UU	26	

Abstract:
An overview of impedance- and modal-based substructure analysis techniques used in the Structural Acoustics Department is presented. The impedance technique described herein offers a substantial advantage over other coupling techniques because it is uniquely suited to handle data sets of varying origin. Of particular interest is the combination of numerically and experimentally derived frequency response data, which is especially useful for analyzing structures comprised of components too complex to model using the finite element technique. The impedance-based method is derived from the frequency domain substructure synthesis algorithm introduced by Jetmundsen *et al* [1], which offers a significant improvement over the traditional frequency domain technique in terms of the processing requirements. The modal-based methods involve the coupling of substructure eigenanalysis results to arrive at coupled system (complex-valued) eigenvectors and allow forced response simulations for the coupled system. This method offers an alternative to traditional techniques employed by commercial finite element codes. Limitations of both techniques are identified and discussed along with potential methods for avoiding these shortcomings. Several example problems are presented that show each method's usefulness.

TABLE OF CONTENTS

LIST OF TABLES

List of Figures

List of Figures

LIST OF SYMBOLS

A = substructure label or acoustic matrix
B = substructure label or damping matrix
C = substructure label
F = force
I = substructure interface set
J = substructure interface set
K = stiffness matrix or substructure interface set
M = mass matrix, a moment, or a Boolean mapping matrix
N = number of degrees of freedom
T = transformation matrix
Y = mobility
Z = impedance
n = matrix size
p = load vector or modal participation factor
r = modal constant
s = linear spacing
u = displacement vector
x = translational coordinate or displacement vector
y = translational coordinate
z = translational coordinate
α = rotational coordinate or degree of freedom set
β = rotational coordinate
ϕ = mode shape array
γ = rotational coordinate or degree of freedom set
η = mechanical loss factor
ω = circular frequency

1 Introduction

Substructure modeling is used to simulate the combined dynamic response of finite element (FE) models for different structures or individual components constituting a larger structure. The main goal of such a method is to improve the reusability of component models and to reduce the system matrix sizes [2]. More recently, the focus of substructuring has shifted to combining FE and experimental results or multiple sets of experimental results for structures that are too complicated to model accurately with the finite element technique [1,3,4].

Numerous substructure coupling techniques have been proposed in the literature. Of these, two main categories emerge: 1) impedance coupling techniques, and 2) modal coupling techniques. The impedance coupling techniques focus on spatial information (mass, stiffness, frequency response functions (FRFs), etc), while the modal coupling techniques employ modal models that can be derived from numerical models or from experimental data. The impedance coupling technique described herein is based on the latest frequency domain substructure synthesis formulation introduced by Jetmundsen *et al* [1]. This method represents an improvement over traditional impedance-based synthesis techniques in that it is far less computationally expensive. The modal coupling technique discussed herein makes use of an eigenvalue solution of the *coupled* system matrices, in modal space, to obtain system eigenvectors. The focus of this report is to document the utility and limitations of both of these coupling techniques.

2 Background

Because the coupling techniques presented herein have developed out of the finite element substructuring domain, a brief overview of finite element substructure modeling[1] is provided [1]. The process involves a division of the structure into smaller components (superelements), which are processed individually to obtain a set of reduced matrices that describe the characteristics of the superelement as seen by the rest of the structure. The reduced matrices for the superelements are combined into a single set of matrices that are solved to obtain the *assembly* solution. (The assembled reduced matrix is sometimes referred to as the *residual structure*.) Results for the assembly solution are then used for the superelement data recovery, during which the transformation matrix used in the reduction step is used to relate information about the coupling degrees of freedom to the superelement internal degrees of freedom. While the matrix reduction theory for static analyses is exact, the reduction process for dynamic analysis requires approximations for both the mass and damping matrices.

The main advantage of substructuring is improved modeling efficiency. It is often the case that a FE model is solved several times, each time with small changes to a portion of the model. With substructuring, only the superelement undergoing a modification and the assembled matrices are solved for a given iteration. Efficiency is also a factor when a model is comprised of many of the same superelements. For example, Figure 2.1 shows a gear that is subdivided according to the symmetry about the axis of rotation. The solid line in this figure shows a single superelement that is replicated around the axis of rotation to make up the gear model. No matrix reductions are required for the imaged elements (shown by the dashed lines in Figure 2.1), and thus substantial time savings are possible for such a model.

---

[1] Finite element substructure modeling is also referred to as *superelement analysis* or simply *substructuring*

The main disadvantage of substructuring is the loss of accuracy for dynamic analyses. As stated above, the dynamic reduction of the mass and damping matrices are only approximate. The approximation arises from the inability to exactly compute the response of the internal nodes due to fixed boundary nodes. The exact computation would require all of the modes for each superelement, which is generally prohibitive. MSC/Nastran offers several methods to perform the dynamic reduction, ranging from a static (Guyan) reduction where the local dynamic effects are ignored, to component modal synthesis (CMS) where dynamic shape functions are used to form a dynamic transformation that is used in conjunction with the static transformation to capture the local dynamic effects. With CMS, different interface conditions can be applied: fixed (also known as the Craig-Bampton method), free, or mixed (fixed and free).

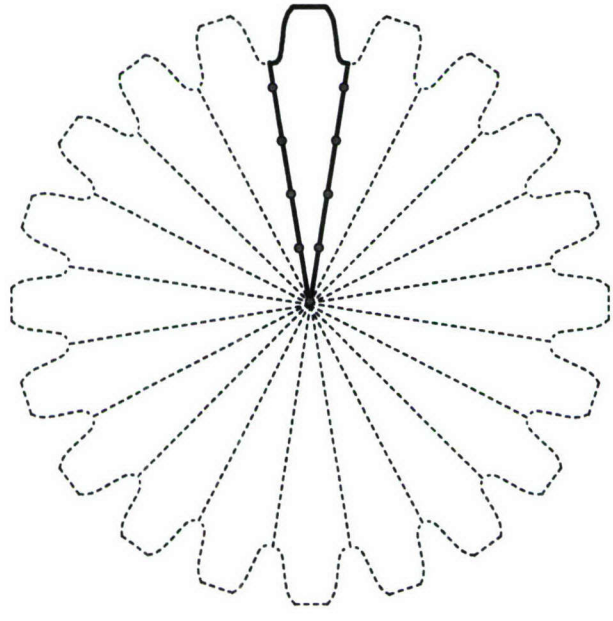

Figure 2.1. Sample FE substructuring for a gear with symmetry about the axis of rotation

The modal coupling technique described below is plagued by the same limitation as substructuring dynamic analysis, namely mode truncation. Effects of mode truncation may also exist in the Frequency Domain Substructure Synthesis (FDSS) technique, but the main limitation of FDSS is generally due to incomplete datasets (i.e., degree of freedom truncation). Both of these techniques and their limitations are described below.

3 Modal Coupling Technique

The modal coupling technique involves generalized mass and stiffness matrices[2], which are obtained by transforming the system matrices (e.g., mass, stiffness, damping, etc.) from spatial to modal coordinates:

$$u = \phi p \,, \tag{1}$$

where u is a displacement vector in the spatial coordinate system, ϕ is the mode shape array, and p is a vector of modal participation factors. Then, by substituting Equation 1 into the equation of motion (Equation 2) and pre-multiplying by ϕ^T yields the generalized matrices, Equation 3. If a

[2] Damping can also be accounted for in the same manner as the mass and stiffness.

numerical model exists (i.e., if the mass and stiffness matrices are known), the mode shapes are determined by performing an eigenanalysis for each substructure.

$$[M]\{\ddot{u}\}+[K]\{u\}=F\,, \tag{2}$$

$$\begin{matrix}[\overline{M}]=[\phi]^T[M][\phi] \\ [\overline{K}]=[\phi]^T[K][\phi]\end{matrix}\,, \tag{3}$$

Obtaining these matrices from experimental data is somewhat more difficult because the mass and stiffness matrices are not known. However, methods are available to approximate the matrices from modal analysis results as shown in Reference 5.

Additional mass (ΔM) and stiffness (ΔK) can be added to the structure, as shown below in Equation 4. (Note that superscripts a and b in Equation 4 refer to separate substructures.) The added stiffness term can represent a coupling stiffness between substructures or can be a single stiffness connected to ground.

$$\left[\left[\begin{array}{c|c}\overline{M}^a & \\ \hline & \overline{M}^b\end{array}\right]+[\phi]^T[\Delta M][\phi]\right]\{\ddot{p}\}+\left[\left[\begin{array}{c|c}\overline{K}^a & \\ \hline & \overline{K}^b\end{array}\right]+[\phi]^T[\Delta K][\phi]\right]\{p\}=0 \tag{4}$$

An eigenanalysis can be performed on Equation 4 to obtain the resonance frequencies and normal modes of the modified structure. However, because structural acoustic predictions are generally focused on obtaining broadband vibration levels due to specific loads, the non-homogeneous version of Equation 4, along with additional matrices for damping (B) and acoustics (A), is solved for specific loads at specific frequencies. The complete matrix equation including the force vector (f) is shown below in Equation 5.

$$\begin{aligned}&\left[\left[\begin{array}{c|c}\overline{M}^a & \\ \hline & \overline{M}^b\end{array}\right]+[\phi]^T[\Delta M][\phi]\right]\{\ddot{p}\}+\left[\left[\begin{array}{c|c}\overline{B}^a & \\ \hline & \overline{B}^b\end{array}\right]+[\phi]^T[\Delta B][\phi]\right]\{\dot{p}\} \\ &+\left[\left[\begin{array}{c|c}\overline{K}^a & \\ \hline & \overline{K}^b\end{array}\right]+[\phi]^T[\Delta K][\phi]+[\phi]^T\left[A(\varpi)\right][\phi]\right]\{p\}=[\phi]^T\{f\}\end{aligned} \tag{5}$$

Complex-valued mode shapes and resonance frequencies for the homogeneous version of Equation 5 are computed using a singular value decomposition (SVD) approach [6] or an eigenanalysis that makes use of a polynomial fit to account for the frequency-dependent acoustic matrix [7,8]. Three of the major advantages to such a procedure include: 1) reduction of the matrix sizes of the second eigenvalue analysis through the use of modal matrices, 2) facilitates the solution of large FE models, as they can be separated into smaller, more manageable problems, and 3) allows for easy implementation of frequency-dependent added mass, stiffness, damping[3], and acoustic matrices. The limitation of this method is the inability to include all modes for all components, which is required for an exact numerical solution. However, the effects of this limitation are often negligible, but must be investigated on a per-model basis via convergence studies. A discussion of mode truncation effects is provided below in Section 4.2.

---

[3] Note that in addition to the viscous damping, B, hysteresis damping can be added through the use of a complex-valued stiffness matrix.

4 FRF Impedance Coupling Techniques

Impedance coupling via frequency response functions requires knowledge of the mobility matrices, Y, for each of the substructures being combined. A mobility matrix for a structure represents the inverse of the structure's impedance matrix ($Y = Z^{-1}$, where Z is the structural impedance), which is defined as follows:

$$\{p\} = [Z] \cdot \{\dot{x}\}, \tag{6}$$

where $\{p\}$ is the load vector and $\{\dot{x}\}$ is the velocity vector.

In general, the mobility matrices are $6N$ x $6N$ complex-valued matrices, where N is the number of DOFs. The mobility matrix for a single DOF is:

$$\begin{Bmatrix} \dot{x} \\ \dot{y} \\ \dot{z} \\ \dot{\alpha} \\ \dot{\beta} \\ \dot{\gamma} \end{Bmatrix} = \begin{bmatrix} Y_{xx} & Y_{xy} & Y_{xz} & Y_{x\alpha} & Y_{x\beta} & Y_{x\gamma} \\ Y_{yx} & Y_{yy} & Y_{yz} & Y_{y\alpha} & Y_{y\beta} & Y_{y\gamma} \\ Y_{zx} & Y_{zy} & Y_{zz} & Y_{z\alpha} & Y_{z\beta} & Y_{z\gamma} \\ Y_{\alpha x} & Y_{\alpha y} & Y_{\alpha z} & Y_{\alpha\alpha} & Y_{\alpha\beta} & Y_{\alpha\gamma} \\ Y_{\beta x} & Y_{\beta y} & Y_{\beta z} & Y_{\beta\alpha} & Y_{\beta\beta} & Y_{\beta\gamma} \\ Y_{\gamma x} & Y_{\gamma y} & Y_{\gamma z} & Y_{\gamma\alpha} & Y_{\gamma\beta} & Y_{\gamma\gamma} \end{bmatrix} \cdot \begin{Bmatrix} F_x \\ F_y \\ F_z \\ M_x \\ M_y \\ M_z \end{Bmatrix}, \tag{7}$$

where the coordinates are defined in Figure 4.1. As shown in Equation 7, 75% of the components in the mobility matrix involve a rotational coordinate, an important detail that will be discussed later.

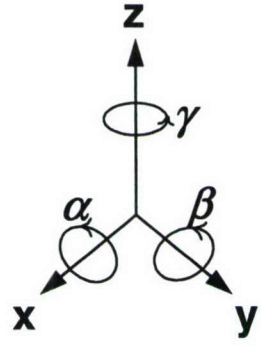

Figure 4.1. Coordinate system used for the definition of the mobility matrix

Mobility matrices similar to the matrix shown in Equation 7 can be defined for all degrees of freedom for each structure that is to be coupled. Furthermore, these matrices can be partitioned according to *internal* and *coupling* DOFs. The partitioned mobility matrices for two substructures, A and B, are shown in Equations 8 and 9.

$$Y^A(\varpi) = \left[\begin{array}{c:c} Y_{ii}^A & Y_{ic}^A \\ \hdashline Y_{ci}^A & Y_{cc}^A \end{array}\right], \tag{8}$$

$$Y^B(\varpi)=\left[\begin{array}{c|c} Y_{ii}^B & Y_{ic}^B \\ \hline Y_{ci}^B & Y_{cc}^B \end{array}\right], \tag{9}$$

The classical derivation of substructure synthesis using FRFs employs impedance matrices instead of mobility matrices [4,5]. With these matrices, displacement compatibility, and force equilibrium at the coupling DOFs:

$$\begin{aligned} u_c^A &= u_c^B \\ F_c^A + F_c^B &= F_c \end{aligned} \tag{10}$$

the following relation for the coupling of substructures A and B can be derived (see Reference 5 for a complete derivation):

$$Y^* = \begin{bmatrix} Z_{ii}^A & Z_{ic}^A & 0 \\ Z_{ci}^A & Z_{cc}^A + Z_{cc}^B & Z_{ci}^B \\ 0 & Z_{ic}^B & Z_{ii}^B \end{bmatrix}^{-1}, \tag{11}$$

where Y^* is the mobility matrix for the coupled system. As seen in this relation, such a coupling process requires three matrix inversions: one for the mobility matrix of substructure A (required to obtain the impedance matrix), one for the substructure B mobility matrix, and a third inversion for assembled matrix. In general, the number of matrix inversions is one greater than the number of substructures being combined. The size of these matrices are n_A x n_A for substructure A, n_B x n_B for substructure B, and n^* x n^* for the combined structure, where $n^* = n_A + n_B - n_C$.

4.1 Generalized FRF Impedance Coupling Technique

The large computation requirements of the FRF coupling relation shown in Equation 11 can be avoided by using the generalized approach developed by Jetmundsen *et al* [1]. The formulation for two substructures, A and B, is shown below in Equation 12 (see Reference 9 for a derivation of this relation):

$$Y^* = \begin{bmatrix} Y_{ii}^A & Y_{ic}^A & 0 \\ Y_{ci}^A & Y_{cc}^A & Y_{ci}^B \\ 0 & Y_{ic}^B & Y_{cc}^B \end{bmatrix} - \begin{bmatrix} Y_{ic}^A \\ Y_{cc}^A \\ Y_{ic}^B \end{bmatrix} \left[Y_{cc}^A + Y_{cc}^B\right]^{-1} \begin{bmatrix} Y_{ic}^A \\ Y_{cc}^A \\ Y_{ic}^B \end{bmatrix}^T. \tag{12}$$

It is apparent from this relation that only a single matrix inversion of size n_C x n_C is required for this coupling algorithm, which is a significant improvement over the classical approach (Equation 11). The theory has been generalized to incorporate Boolean mapping matrices, called connectivity matrices [9], that define the structural interconnections. The generalized relation is shown below in Equation 13.

$$Y^* = Y_{\alpha\alpha} - \left[M \otimes Y_{\alpha\gamma}\right] \cdot \left[\sum_{q=1}^{N} M_q^T M_q \otimes Y_{\gamma\gamma}^q\right]^{-1} \cdot \left[M \otimes Y_{\alpha\gamma}\right]^T, \tag{13}$$

where M is the Boolean mapping matrix defining the interfacial sign convention for the coupling forces and their reactions, α is a substructure identifier in addition to a set of internal DOFs, γ is an interface identifier that implies an interface DOF set, $\otimes$ represents a matrix element-by-

element multiplication, and N is the number of substructures. The notation is best understood with the use of an example.

Consider the structure shown in Figure 4.2, which consists of three substructures—A, B, and C—and three interfaces—I, J, and K. Each column of the mapping matrix corresponds to an interface, while each row corresponds to a substructure. A positive direction is arbitrarily assigned to each interface, as shown by the positive and negative signs adjacent to the interface arrows in Figure 4.2. The arbitrary sign convention is applied to the interfaces for the purpose of constructing the mapping matrix. For each substructure (i.e., each row of the matrix), a "+1" or "-1" is placed in the columns corresponding to an interface that connects to the substructure. The decision to use a "+1" or "-1" is based upon the chosen sign convention. The mapping matrix corresponding to the structure in Figure 4.2 is as follows:

$$M = \begin{matrix} \\ A \\ B \\ C \end{matrix} \begin{matrix} \begin{matrix} I & J & K \end{matrix} \\ \begin{bmatrix} 1 & -1 & 0 \\ -1 & 0 & 1 \\ 0 & 1 & -1 \end{bmatrix} \end{matrix}. \tag{14}$$

The mobility matrix, $Y_{\alpha\alpha}$, is defined as follows:

$$Y_{\alpha\alpha} = \begin{bmatrix} Y_{aa}^{A} & 0 & 0 \\ 0 & Y_{bb}^{B} & 0 \\ 0 & 0 & Y_{cc}^{C} \end{bmatrix}, \tag{15}$$

where a represents the internal degrees of freedom for substructure A, b are the internal degrees of freedom for substructure B, and so on. These DOF sets are the DOFs for which mobility information will be computed in the synthesized mobility matrix. If response information is required for any of the interface degrees of freedom, they can be combined in these DOF sets. However, each interface DOF can only reside in one set. For instance, if results are required for the interface DOFs associated with the I interface, these DOF can be included in either the a or

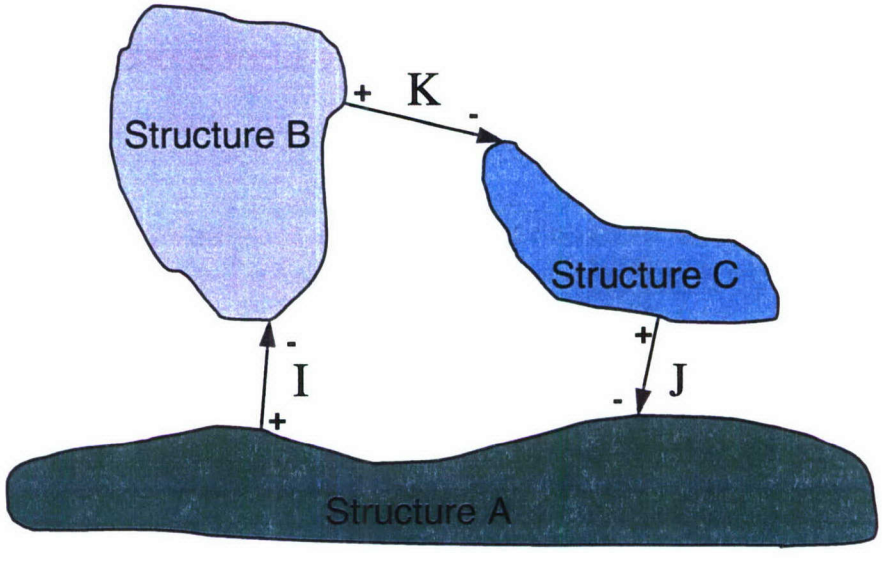

Figure 4.2. Frequency domain substructure synthesis diagram

the b set, but not both. Note that the order of the DOF sets in $\alpha = \{a, b, c\}$ correspond to the order of the substructures in the rows of the mapping matrix (Equation 14). The cross mobility matrix between interface and internal DOFs is defined as follows:

$$Y_{\alpha\gamma} = \begin{bmatrix} Y_{ai}^{A} & Y_{aj}^{A} & Y_{ak}^{A} \\ Y_{bi}^{B} & Y_{bj}^{B} & Y_{bk}^{B} \\ Y_{ci}^{C} & Y_{cj}^{C} & Y_{ck}^{C} \end{bmatrix}. \tag{16}$$

Here, the i, j, and k DOF sets represent the DOFs associated with the I, J, and K, interfaces, respectively. The order of the interface DOF sets, $\gamma = \{i, j, k\}$, corresponds to the columns of the mapping matrix (Equation 14). When multiplied by the mapping matrix, M, using an element by element multiplication, some of the components in this matrix are nullified (e.g., Y_{ak}^{A} becomes zero because the K interface does not contact the A substructure):

$$M \otimes Y_{\alpha\gamma} = \begin{bmatrix} 1 & -1 & 0 \\ -1 & 0 & 1 \\ 0 & 1 & -1 \end{bmatrix} \otimes \begin{bmatrix} Y_{ai}^{A} & Y_{aj}^{A} & Y_{ak}^{A} \\ Y_{bi}^{B} & Y_{bj}^{B} & Y_{bk}^{B} \\ Y_{ci}^{C} & Y_{cj}^{C} & Y_{ck}^{C} \end{bmatrix} = \begin{bmatrix} Y_{ai}^{A} & -Y_{aj}^{A} & 0 \\ -Y_{bi}^{B} & 0 & Y_{bk}^{B} \\ 0 & Y_{cj}^{C} & -Y_{ck}^{C} \end{bmatrix}. \tag{17}$$

The final part of Equation 13 that requires explanation is the summation term:

$$\sum_{q=1}^{N} M_q^T M_q \otimes Y_{\gamma\gamma}^{q}. \tag{18}$$

Here, a subscript of the mapping matrix represents a row of the matrix. For this example, M_1 = [1 -1 0]. The summation from $q = 1$ to N is a summation over the substructures, where the order corresponds to the rows of the mapping matrix (e.g., q = 1 is the first row of M which corresponds to substructure A, q = 2 is the second row of M which corresponds to substructure B, and so on). With this definition, we have $Y_{\gamma\gamma}^{1} = Y_{\gamma\gamma}^{A}$ where γ is the internal DOF set previously defined.

While the theory described here for performing substructure synthesis analyses is exact, the accuracy is often limited by shortcomings of the mobility matrices. These deficiencies can be a result of numerous sources. The most common sources are mode truncation and lack of rotational degrees of freedom (RDOFs) information. Both of these sources of error are discussed next.

4.2 Mode Truncation Effects

Mode truncation errors are a result of generating frequency response functions from an incomplete modal database.[4] This database can be derived from either a numerical model or experimental measurements. In any case, the errors result from using only a partial set of eigenvalues in a modal summation solution for a system's response. For example, a finite element model may consist of N DOFs from which N mode shapes can be derived. However, due to practical limitations, usually only the first M modes are retained ($M < N$). Such a truncation generally has a negligible effect on the resonance frequencies, but does shift the

[4] When FRFs are used in their "as measured" state, there is no modal truncation error associated with the data.

antiresonances *upward* in frequency. (The reason for the upward shift in antiresonance frequency can be explained by considering the residual term that is discussed later.) While this effect may have a negligible impact on most applications of the FRFs, substructure synthesis methods can be particularly sensitive to this type of effect [3,5].

The mode truncation effect is shown below in Figure 4.3, which shows results from modal summation solutions for a cantilever beam finite element model. The figure indicates the increased error associated with the point FRF at the tip of the beam (i.e., the free end) as the number of summed modes decreases from $N = M = 14$ to $M = 3 < N$. Because it is often not practical to use all possible mode shapes in solutions due to memory limitations for numerical modes or measurement limitations for experimental modes (limited to a finite upper frequency), the effect of the truncated modes can be approximated with the use of *residual* terms [5]. These terms are used to account for truncation of both 'low-frequency' and 'high-frequency' modes. As described by Ewins [5], the truncated low-frequency modes exhibit a mass-like behavior while the high-frequency modes exhibit a stiffness-like behavior. If the modal summation is represented in terms of the modal parameters (resonance frequencies (ω_r), damping (η_r), and modal constants ($r^{A_{jk}}$) for a general mobility between points j and k), the modal summation has the following form:

$$Y_{jk}(\varpi) = -\frac{i}{\varpi M_{jk}^{R}} + \sum_{r=m_1}^{m_2} \frac{i\varpi r^{A_{jk}}}{\varpi_r^2 - \varpi^2 + i\eta_r\varpi_r^2} + \frac{i\varpi}{K_{jk}^{R}}, \tag{19}$$

where M_{jk}^{R} is the residual mass, K_{jk}^{R} is the residual stiffness, m_1 is one larger than the number of truncated low-frequency modes, and m_2 is the number of modes included in the modal summation *plus* the number of truncated low-frequency modes. Methods to estimate these terms can be found in Reference 5. Commercial finite element solvers also may offer methods to

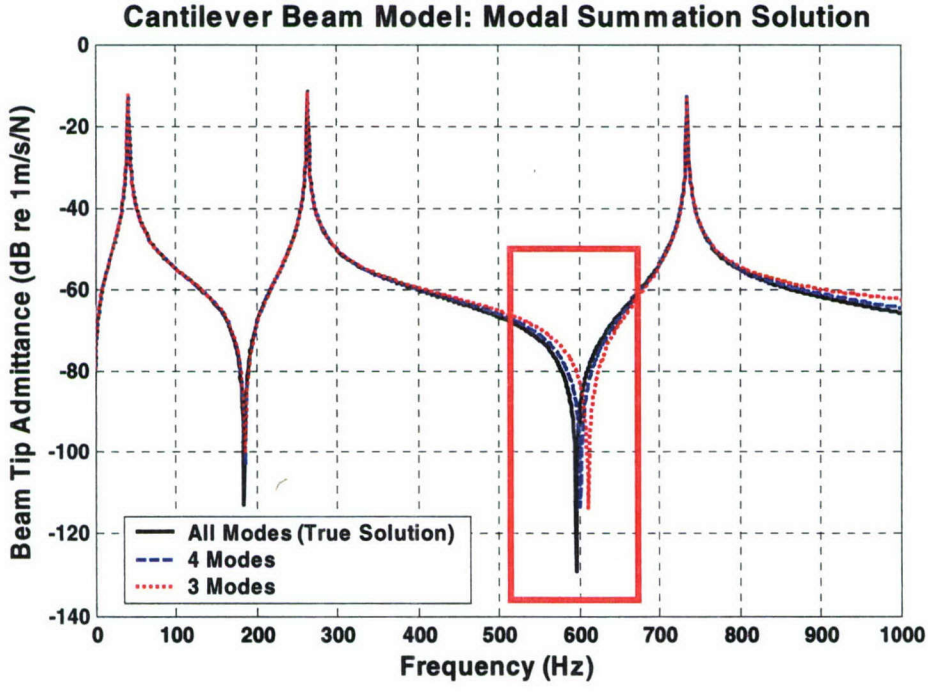

Figure 4.3. Modal summation study showing mode truncation effects

account for the residual terms when performing a numerical modal summation solution. MSC/NASTRAN, for example, can compute a residual vector for each load condition to account for the truncated modes by including the bulk data entry: PARAM,RESVEC,YES. The process involves a static solution of the model to obtain deflection shapes that are then modified or discarded to make them linearly independent of the mode shapes. The residual vectors are computed and appended to the mode shape array.

4.3 Rotational Degree of Freedom Estimation

The second major source of error in frequency response function coupling is associated with neglecting components of the mobility matrices. Often the components not included are the mobilities associated with rotational coordinates. As discussed previously, 75% of the complete mobility matrix involves a rotational coordinate. The importance of these mobilities depends on the components being coupled and the interface DOF placement. For example, a structure with a broad interface that is connected using several DOFs, such as the structure shown in Figure 4.4a, may not require the use of the rotational terms [4], whereas a structure that has collinear interface DOFs (see Figure 4.4b) may require rotational terms about the collinear axis. If the connecting substructure is not amenable to using a broad placement of coupling DOFs then rotational DOF (RDOF) mobilities will be required.

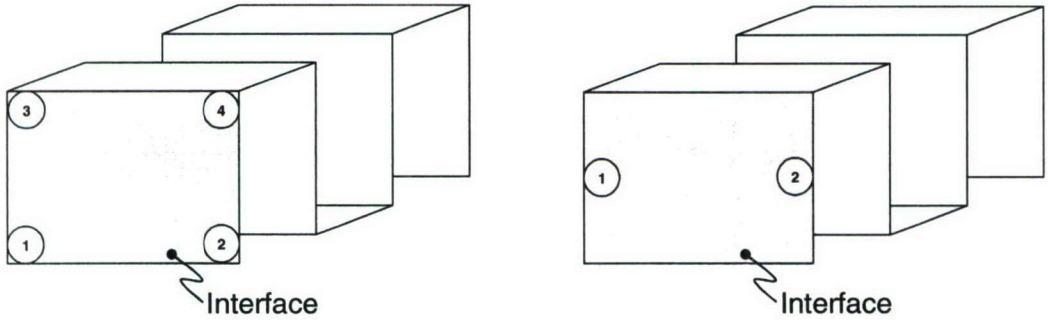

Figure 4.4. Choices of interface DOFs to mitigate effects of not including RDOF mobilities: (a) interface DOFs may adequately capture rotational effects, and (b) collinear DOF placement may require RDOF mobilities

Rotational DOF mobilities are usually neglected due to the difficulty associated with measuring rotational moments and accelerations at a point. While various attempts have been made to develop an accurate method for measuring these mobilities, the most commonly used approach is to infer the rotational information from measured translational information using a finite difference approach [10]. ANSI S2.34-1984 [11] defines standard methods for measuring or estimating the RDOF mobilities using either translational measurements or rotational measurements involving specialized fixtures. A compact implementation of the direct methods of this standard (i.e., the finite difference approach) has been implemented by Duarte and Ewins [10].

The direct method for estimating RDOF mobilities involves the measurement of translational point and cross mobilities as shown in Figure 4.5. The number of required measurements is

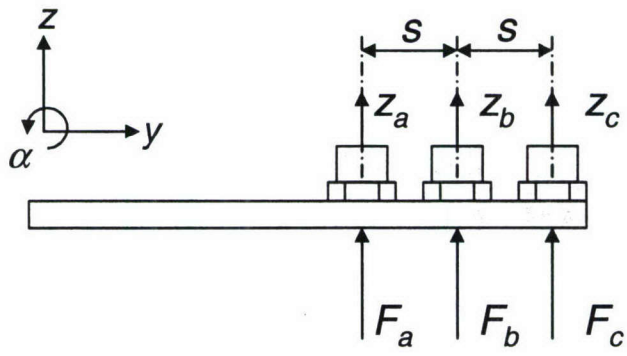

Figure 4.5. Translational mobility measurements for the finite difference RDOF approximation

governed by the desired accuracy of the results. The order of accuracy[5] is one less than the number of measurement points when the traditional finite difference formulae are employed. For example, first order accuracy requires the measurement of mobilities for two locations, second order requires three locations, and so on. As stated earlier, Duarte and Ewins have developed a compact implementation of the finite difference approach. Their method employs the following relation:

$$Y_{est} = \begin{bmatrix} Y_{zz} & Y_{z\alpha} \\ Y_{z\alpha}^T & Y_{\alpha\alpha} \end{bmatrix} = [T][Y_{meas}][T]^T, \tag{20}$$

where Y_{meas} is the measured mobility matrix, Y_{est} is the estimated mobility matrix containing rotational DOF terms, and T is the transformation matrix that is defined according to the approximation order. Transformation matrices for first and second order schemes are shown in Table 4.1. These matrices require a constant spacing of the measurement locations similar to the spacing shown in Figure 4.5. The forward and backward differencing schemes shown in this table are required for estimating mobility information at the edges of a structure. Transformation matrices for unequal spacing and approximation orders other than first or second can be

Table 4.1. First and Second order finite difference transformation matrices

	First Order	Second Order
Forward	$\begin{bmatrix} 0 & 1 \\ 1/s & -1/s \end{bmatrix}$	$\frac{1}{2s}\begin{bmatrix} 0 & 0 & 2s \\ -1 & 4 & -3 \end{bmatrix}$
Central	N/A	$\frac{1}{2s}\begin{bmatrix} 0 & 2s & 0 \\ -1 & 0 & 1 \end{bmatrix}$
Backward	$\begin{bmatrix} 0 & 1 \\ -1/s & 1/s \end{bmatrix}$	$\frac{1}{2s}\begin{bmatrix} 0 & 0 & 2s \\ 1 & -4 & 3 \end{bmatrix}$

[5] The prediction accuracy is related to the sample spacing as follows: N^{th} order has accuracy on the order of s^N, where s is the sample spacing.

developed using the general approach described in Reference 11. Reference 11 relates the RDOF and translational mobilities in terms of the partial derivatives of the translational mobility at the point of interest. Formulae to approximate the partial derivatives are then developed based on the finite difference approach.

5 Illustrative Problems

5.1 Numerical Example of Rotor-Bearing-Stator System Modes Using Substructuring

The following example of a rotor/stator structure will be used to demonstrate the substructuring approach using component modes (referred to below as Component Modes Synthesis, or CMS). For this example, three Nastran normal modes solutions are required: one solution for the rotor model, one solution for the stator model, and one solution of the combined model[6] for validation purposes. In the combined model, springs are used to couple the rotor and stator through translation[7] at grids 1 and 2 and grids 3 and 4 as shown in Figure 5.1. These grids are also used to couple the rotor and stator for substructure analysis. The coupling stiffness matrix is obtained by first considering a simple spring connecting two grids in three translational directions, as shown in Figure 5.2.

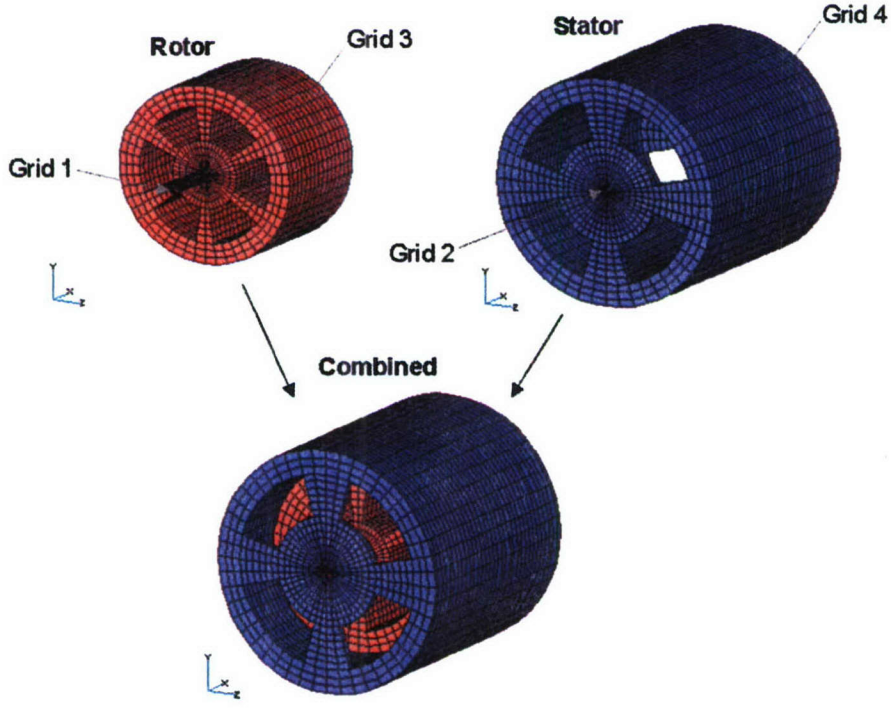

Figure 5.1. Example rotor/stator structure for component mode synthesis example

[6] A normal modes solution is possible here because all matrices (including the added stiffness matrix) are symmetric.

[7] While only translational degrees of freedom are considered here, rotational degree of freedom coupling is often required (e.g., most rolling element bearings have stiffness in all degrees of freedom except rotation about the shaft centerline axis).

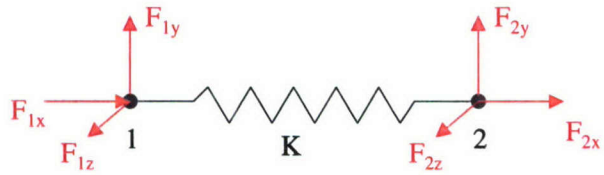

Figure 5.2. General stiffness component free body diagram

Application of a force balance and Hooke's law to the system in Figure 5.2 yields the following set of linear equations:

$$\begin{aligned} F_{1x} &= k_{xx}(x_1 - x_2) + k_{xy}(y_1 - y_2) + k_{xz}(z_1 - z_2) = -F_{2x} \\ F_{1y} &= k_{yx}(x_1 - x_2) + k_{yy}(y_1 - y_2) + k_{yz}(z_1 - z_2) = -F_{2y}, \\ F_{1z} &= k_{zx}(x_1 - x_2) + k_{zy}(y_1 - y_2) + k_{zz}(z_1 - z_2) = -F_{2z} \end{aligned} \tag{21}$$

or in matrix form:

$$\begin{Bmatrix} \vec{F}_1 \\ \vec{F}_2 \end{Bmatrix} = \begin{bmatrix} K & -K \\ -K & K \end{bmatrix} \cdot \begin{Bmatrix} \vec{u}_1 \\ \vec{u}_2 \end{Bmatrix}, \tag{22}$$

where

$$\vec{F}_i = \begin{Bmatrix} F_{ix} \\ F_{iy} \\ F_{iz} \end{Bmatrix} = Force\ \ Vector$$

$$K = \begin{bmatrix} k_{xx} & k_{xy} & k_{xz} \\ k_{yx} & k_{yy} & k_{yz} \\ k_{zx} & k_{zy} & k_{zz} \end{bmatrix} = Stiffness\ \ Matrix. \tag{23}$$

$$\vec{u}_i = \begin{Bmatrix} x_i \\ y_i \\ z_i \end{Bmatrix} = Displacement\ \ Vector$$

A similar expression exists for a general viscous damping element, except that the displacement vector, $\vec{u}$, is replaced by a velocity vector, $\dot{\vec{u}}$. The stiffness matrix shown in Equation 23 is applied to Equation 4 through ΔK.

The details of the structure of Figure 5.1 are:

Stator Width: 1.0 m	Stator Outside Diameter: 1.0 m
Rotor Width: 0.5 m	Rotor Outside Diameter: 0.78 m
Material: Steel	Material Loss Factor: 0.005

The rotor and stator are coupled at both rotor shaft ends via a stiffness coupling matrix, K, representative of a FAFNIR 215k deep groove ball bearing (with the rotational terms neglected here for demonstration purposes):

$$K = \begin{bmatrix} 3.8E6 - i1.9E4 & 2.3E7 - i1.15E5 & -2.3E6 + i1.15E4 \\ 2.3E7 - i1.15E5 & 1.9E8 - i9.5E5 & -1.6E7 + i8.0E4 \\ -2.3E6 + i1.15E4 & -1.6E7 + i8.0E4 & 2.1E7 - i1.05E5 \end{bmatrix}.$$

This coupling matrix is derived from a Hertzian contact stress model for the 215k bearing. The procedure for deriving this matrix is summarized in Reference 12. Note that 1) the imaginary terms in this matrix represent the 0.005 structural loss factor used throughout the model, and 2) units are N/m, N/rad, or N·m/rad.

Resonance frequencies and surface admittances are computed for the Nastran model and the CMS approach. The surface admittances are a result of the coherent dynamic loads (equal magnitude but opposite direction applied to the rotor and stator surfaces) shown by the arrows in Figure 5.3. The CMS results are computed using four sets of basis functions. The first set contains modes up to 659 Hz (25 *total* modes – rotor and stator combined), the second set contains modes to 1.659 kHz (50 *total* modes), the third set contains modes to 2.822 kHz (100 *total* modes), and the final set contains modes extracted separately for the rotor and stator with a total of 100 rotor modes (frequencies up to 6.620 kHz) and 100 stator modes (frequencies up to 3.386 kHz). The Nastran surface admittance was computed using a modal frequency response with a basis set consisting of frequencies up to 2.822 kHz (100 modes).

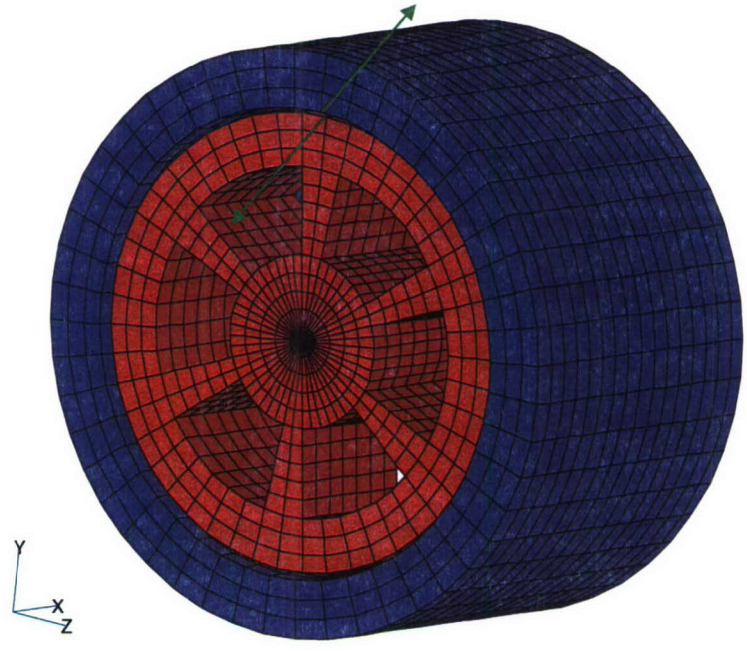

Figure 5.3. Dynamic loads applied to cutaway rotor/stator model

The results of this study show a maximum percent error of less than 2% between the CMS resonance frequencies and the Nastran resonance frequencies. As shown in Figure 5.4, the results do improve as the number of modes included in the CMS basis set increases. Expanding the modal basis set to include 100 rotor modes and 100 stator modes further reduces the error to

around 0.5%. Because of the relatively *soft* rotor/stator coupling used in this example, resonance frequencies above 50. Hz are identical between the Nastran and CMS results.

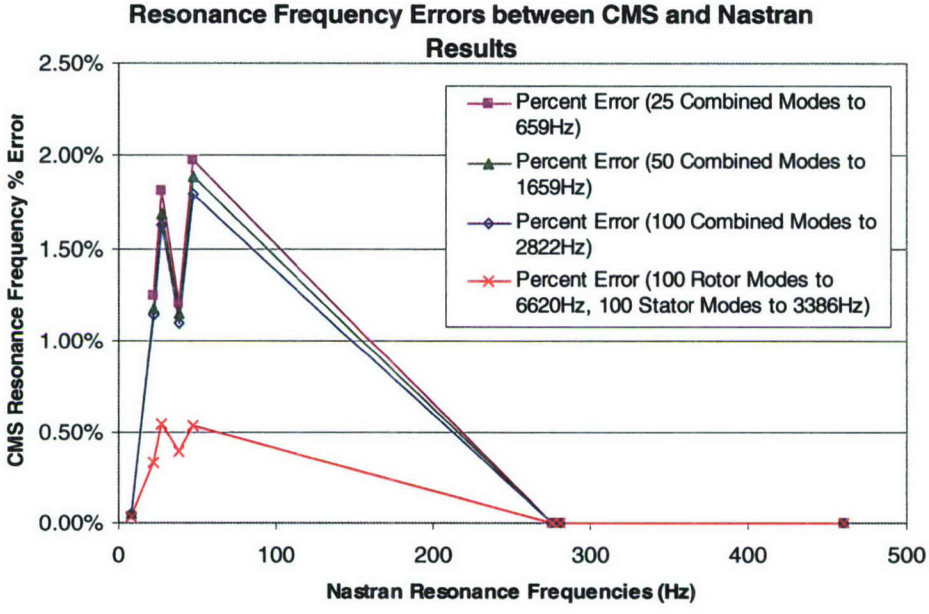

Figure 5.4. CMS versus Nastran coupled rotor/stator resonance frequencies

As shown in Figure 5.5, the computed surface averaged admittances due to the coherent loads shown in Figure 5.3 agree well between the CMS- and Nastran-generated results. However, some differences are apparent in the amplitudes at the resonance frequencies below ~50 Hz. These differences are highlighted in Figure 5.6, where results obtained using CMS with modes up to 2822. Hz are also shown. This figure suggests further improvements in the admittance results are possible if the basis set was expanded to include additional modes.

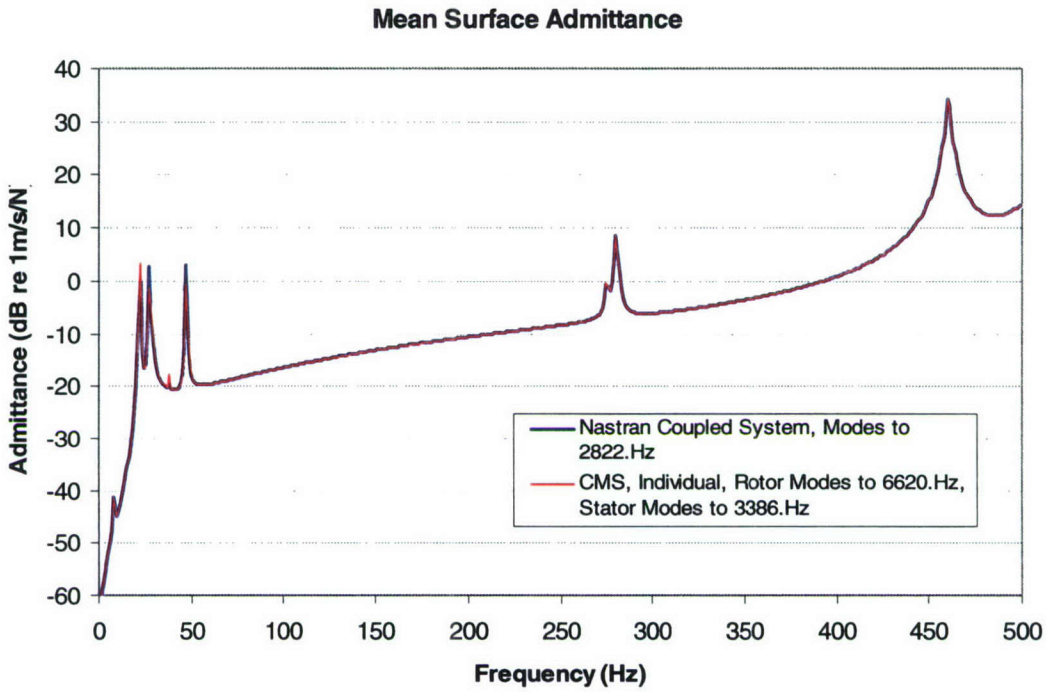

Figure 5.5. Mean surface admittance using CMS-applied bearing stiffnesses and Nastran-applied bearing stiffnesses

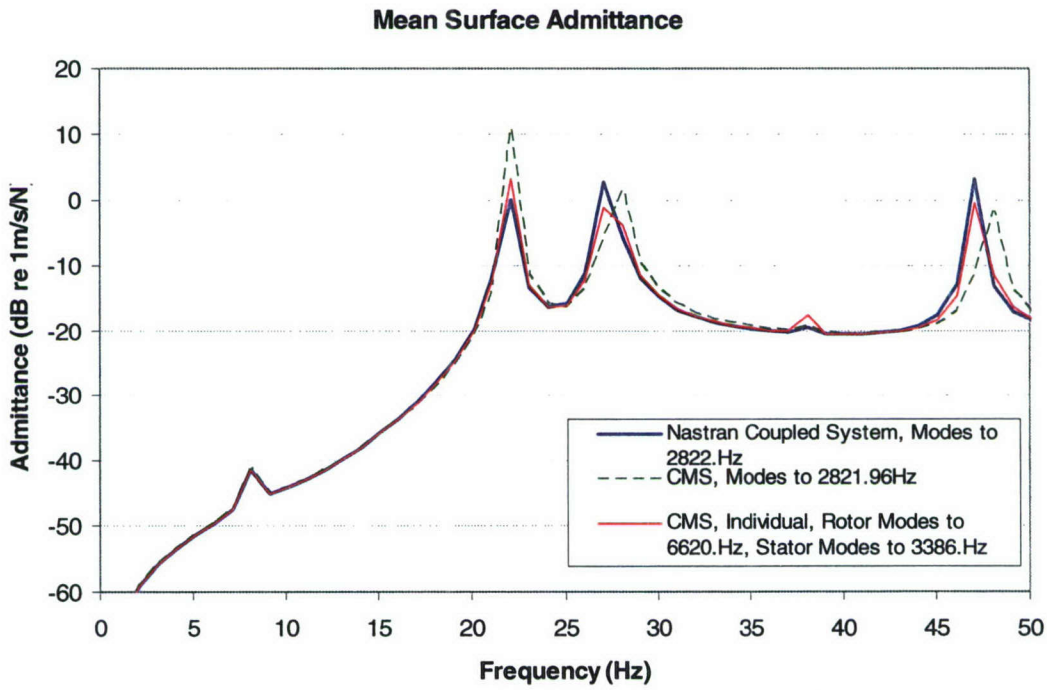

Figure 5.6. Mean surface admittance highlighting region of largest discrepancy

5.2 Numerical Example of Plate and Mass Attachments using FDSS

The synthesis of the combined response of a plate (substructure 0) and two masses (substructures 1 and 2) has been performed using the Jetmundsen algorithm. For this problem, the substructure mobilities were determined from direct frequency response solutions using MSC/NASTRAN (sol 108). The substructures are modeled with quad elements and thus have no mobilities for the drilling DOFs. The models are shown in Figure 5.7. Details regarding the FE model can be found in Reference 13.

The results of the synthesis process are provided in Figure 5.8. This figure shows the admittance for an interface node prior to and after the synthesis process. In addition, the response for the combined model calculated using a direct frequency response with MSC/NASTRAN (i.e., the "true" solution) is also provided in this figure. The results for this synthesis are within round off error to the NASTRAN results. Note that the synthesis process for this example incorporated all of the five available DOFs. Because there are 4 interface nodes, each with 5 DOFs, the solution process required the inversion of a 20x20 matrix at each solution frequency.

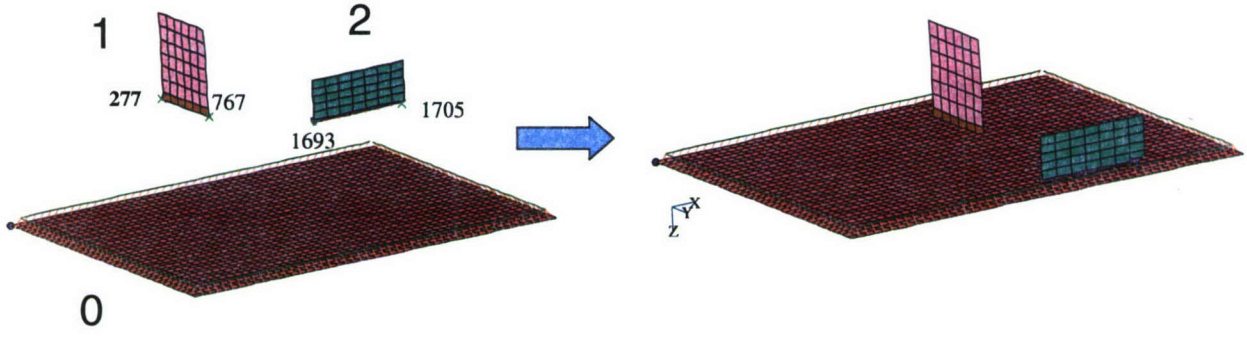

Figure 5.7. Finite element models of example structure prior to and after combining

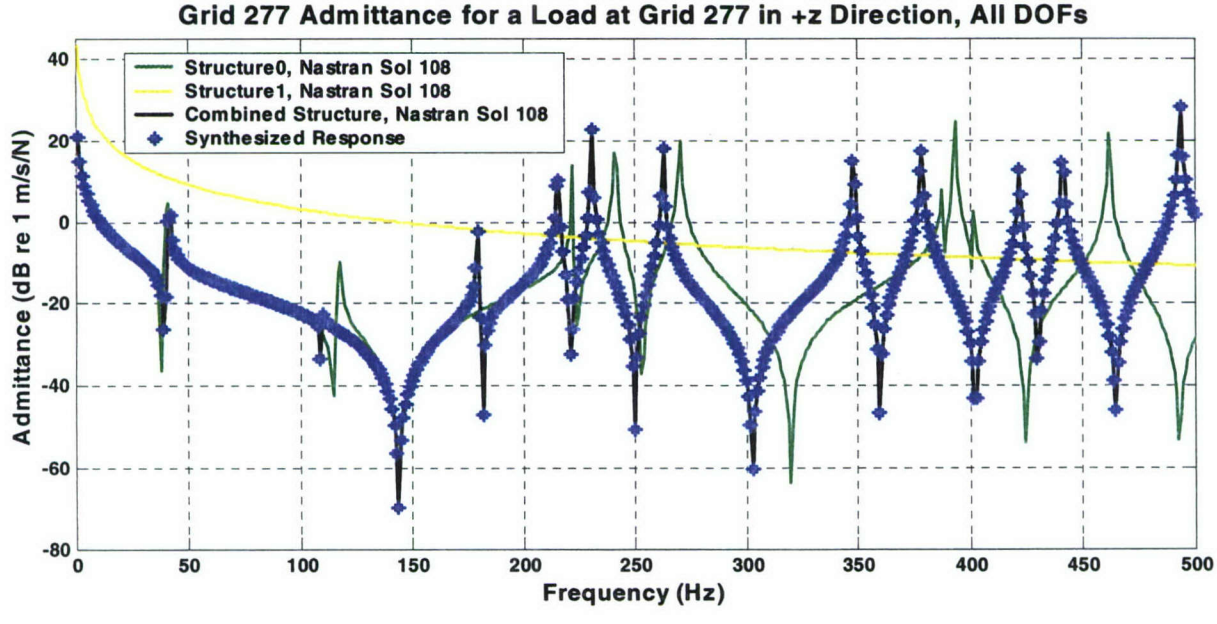

Figure 5.8. Synthesis results for numerical model of plate and mass-like attachments

5.3 Examples of Numerical Plate and Experimental Attachments

5.3.1 Thin Plate Loaded with Electrical Equipment

As stated previously, the frequency domain substructure synthesis technique is aptly suited to accommodate experimental, numerical, or any combination of these data sources. The present example incorporates experimental results for two electrical components that are attached to an edge-stiffened plate as shown in Figure 5.9. The plate mobilities are determined from the same finite element model used in the previous example, while the equipment mobilities are obtained experimentally using an impact hammer and an accelerometer. The details of these components and of the plate FE model can be found in Reference 13.

An attempt to improve the synthesis results was made by adjusting the numerical resonance frequencies of the bare plate to match those determined experimentally. This process involved an identification step wherein the numerical and experimental modes were matched based on a modal assurance criteria (MAC) analysis (see Reference 13) between the numerical eigenanalysis results and the results from a modal analysis of experimental data for the bare, edge-stiffened plate. The numerical resonance frequencies and modal damping levels were then adjusted to match the experimental results. The result of this process is a model that accurately represents the dynamic characteristics of the bare plate up to a frequency of 500 Hz. The mean admittance for the experimental and numerical results due to a normal drive point located at one of the interface grid locations is shown in Figure 5.10. As indicated by this figure, the modified numerical and experimental data sets agree well in terms of resonance frequency location and peak amplitude.

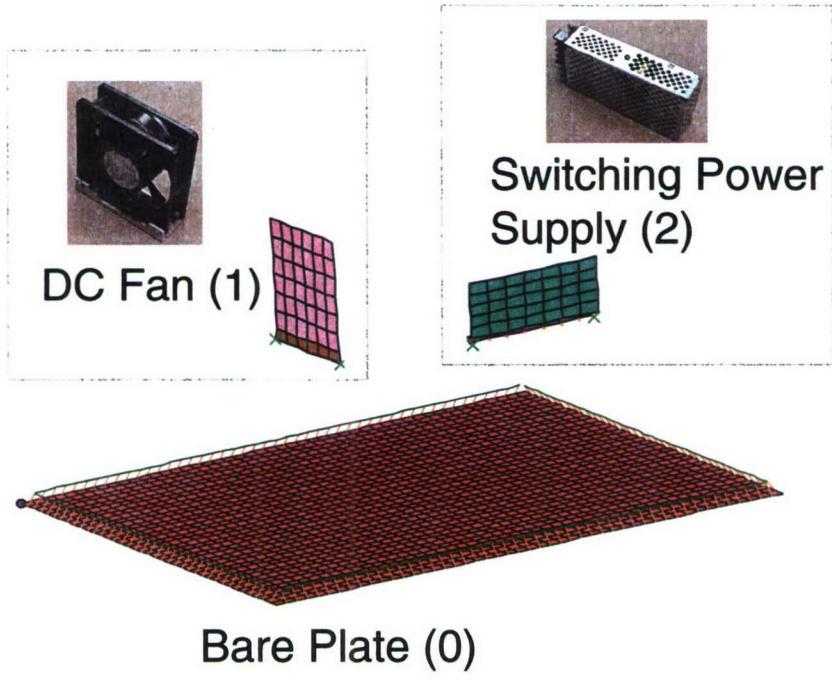

Figure 5.9. Substructure components for synthesis example combining numerical and experimental results

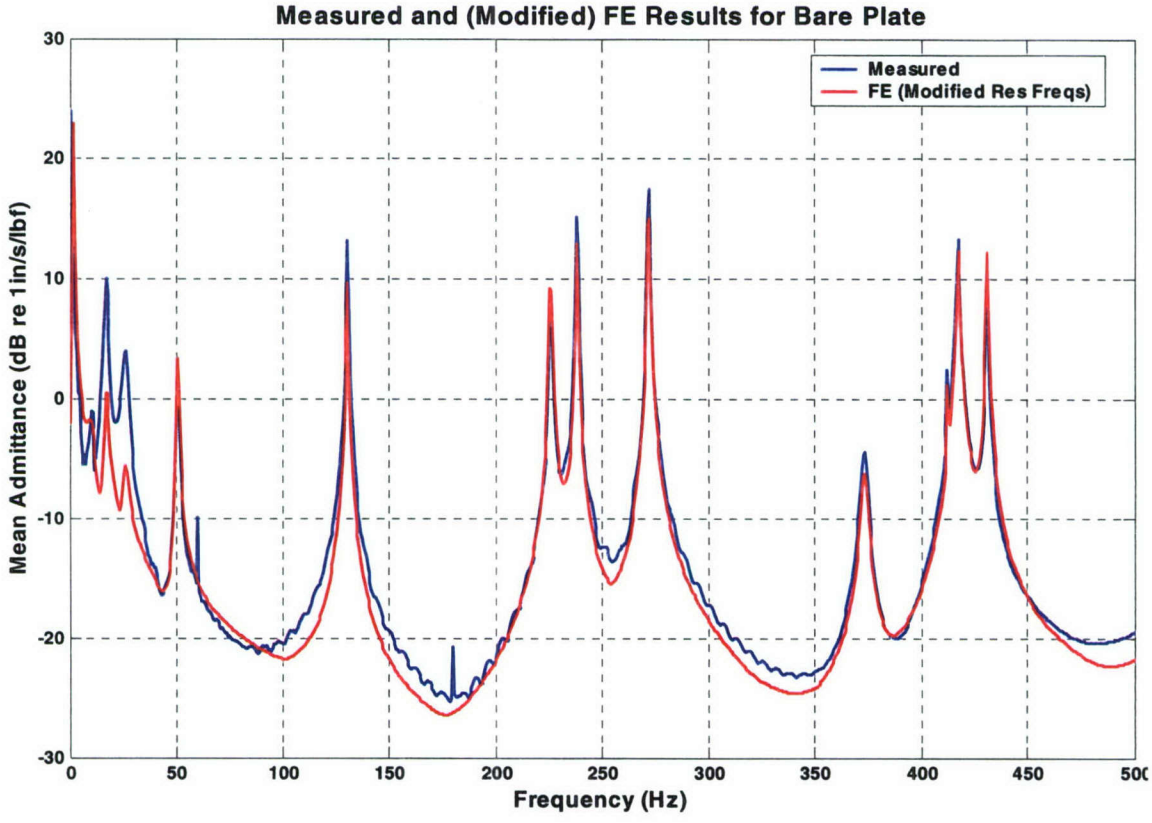

Figure 5.10. Mean measured and predicted admittances for bare, edge-stiffened plate

Point and cross mobilities for all translational degrees of freedom are measured for both attachments using node locations at the four corners on the component interface as shown in Figure 5.11. Components of the resulting mobility matrices are shown in Figure 5.12 for the DC fan and in Figure 5.13 for the switching power supply. The plots in these figures exhibit the transfer function reciprocity property in that the mobility matrices qualitatively show symmetry. It should be noted that the low frequency resonances (approximately less than 50 Hz) are the structure rigid body modes that result from resting the structures on bubble wrap during the testing.

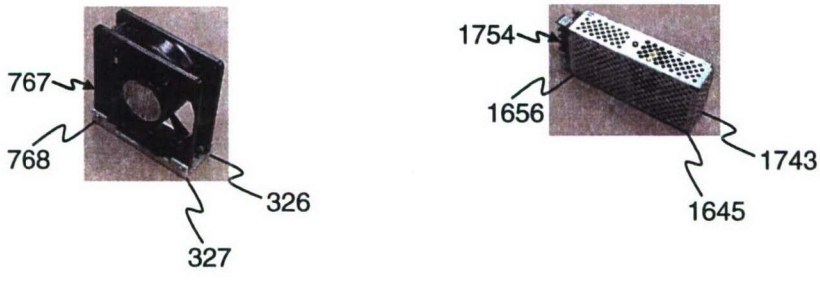

(a) (b)

Figure 5.11. Mobility measurement locations for: (a) the DC Fan and (b) the switching power supply. The numbers correspond to the finite element node IDs at the connection points

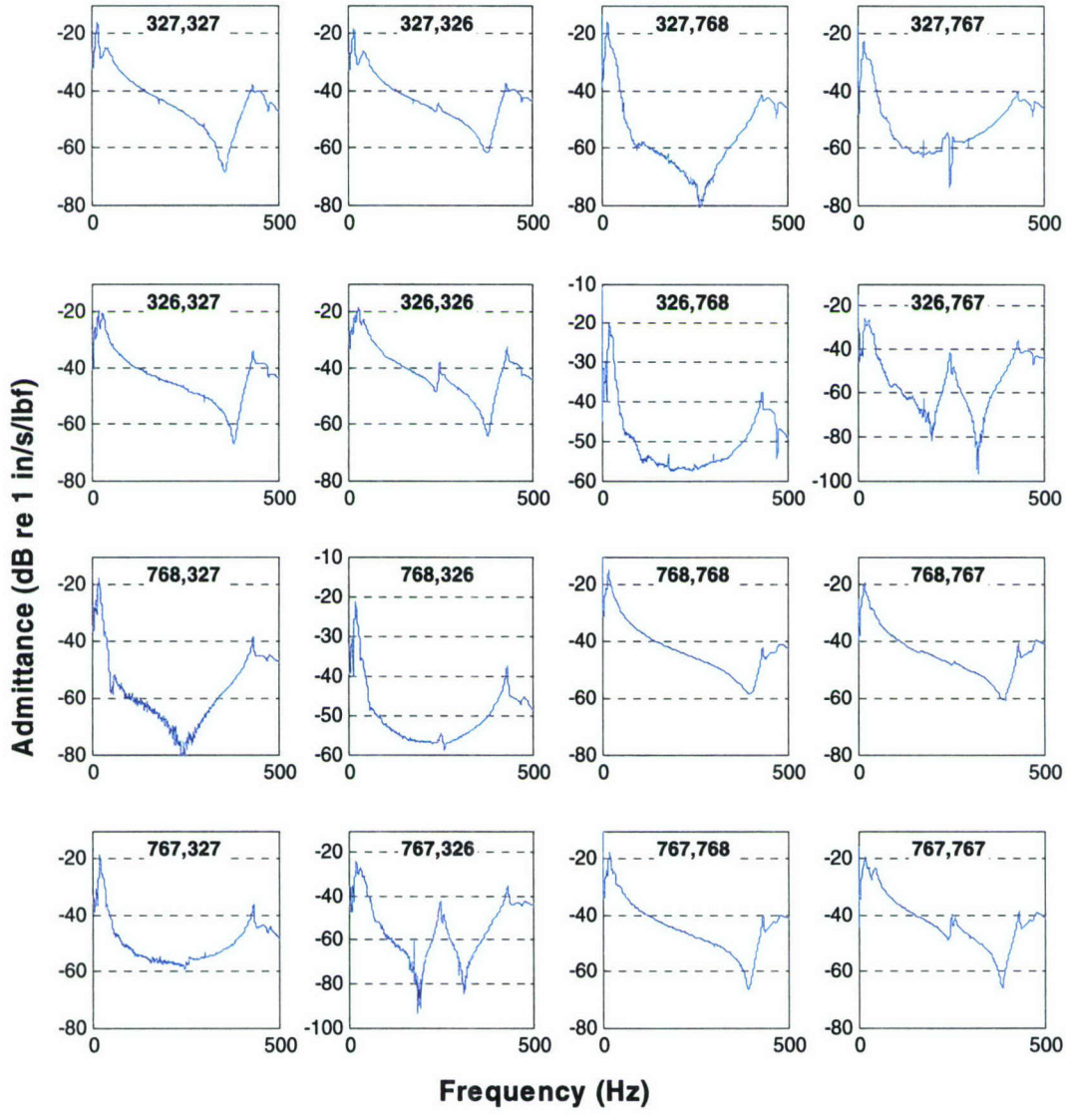

Figure 5.12. DC fan mobility matrix components (referenced to the grid numbers shown in Figure 5.11a)

The mobility of the combined structure is obtained by combining the attachment mobilities with the bare plate mobilities obtained from the numerical model. The same mobility is obtained experimentally by attaching the equipment to the plate using adhesive along with small flat washers at the four mounting locations of each component. (The purpose of the small washers is to create a point-like attachment.) The results of both data sets are provided in Figure 5.14. These results show a similar shift in both resonance locations and amplitudes between the measurements and predictions when the equipment is attached to the bare plate. Note that these results ignore the effect of rotational mobilities because of the difficulty associated with

measuring or predicting these components for such narrow interface surfaces. The following example incorporates the use of a full mobility matrix for the attached structure.

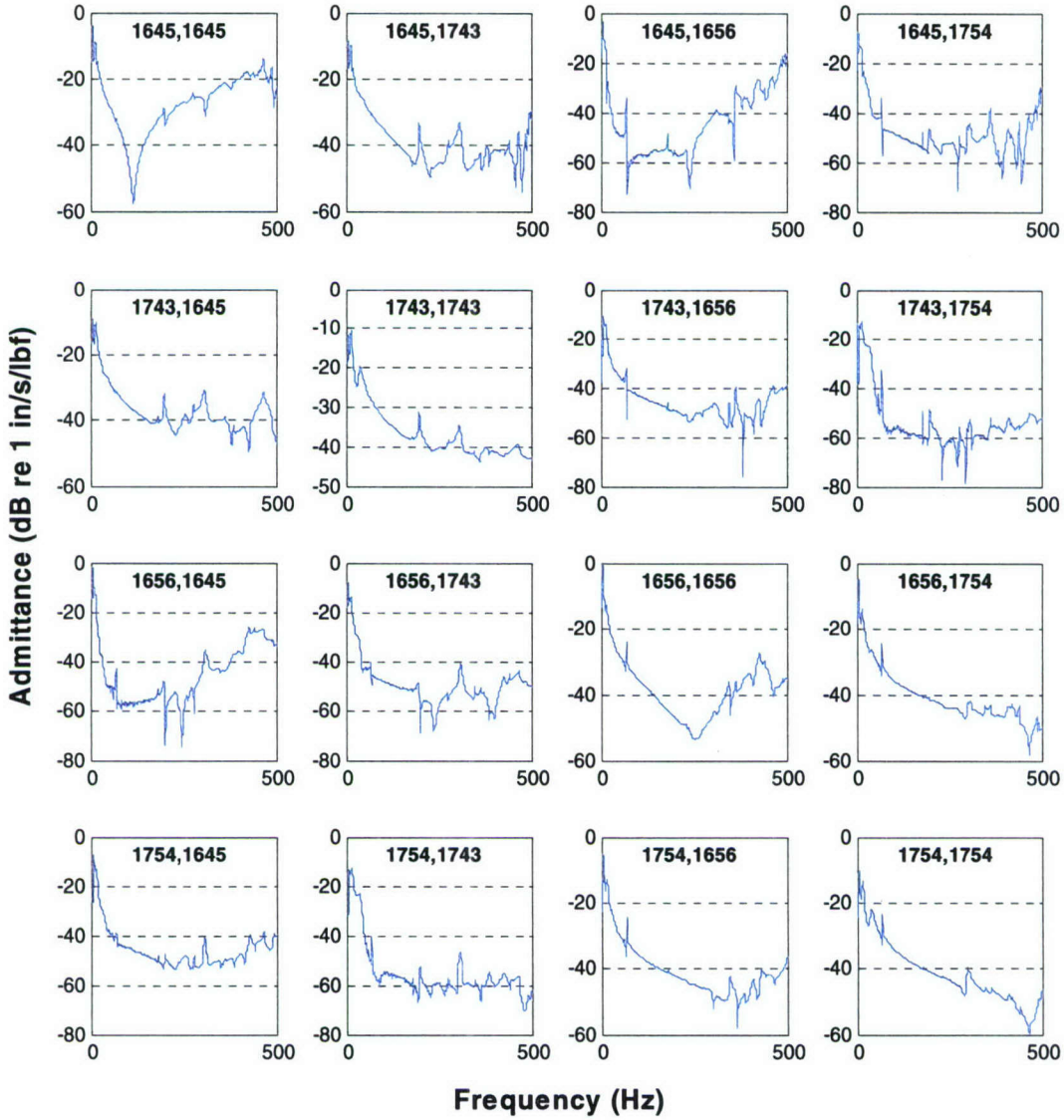

Figure 5.13. Switching power supply mobility matrix components (referenced to the grid numbers shown in Figure 5.11b)

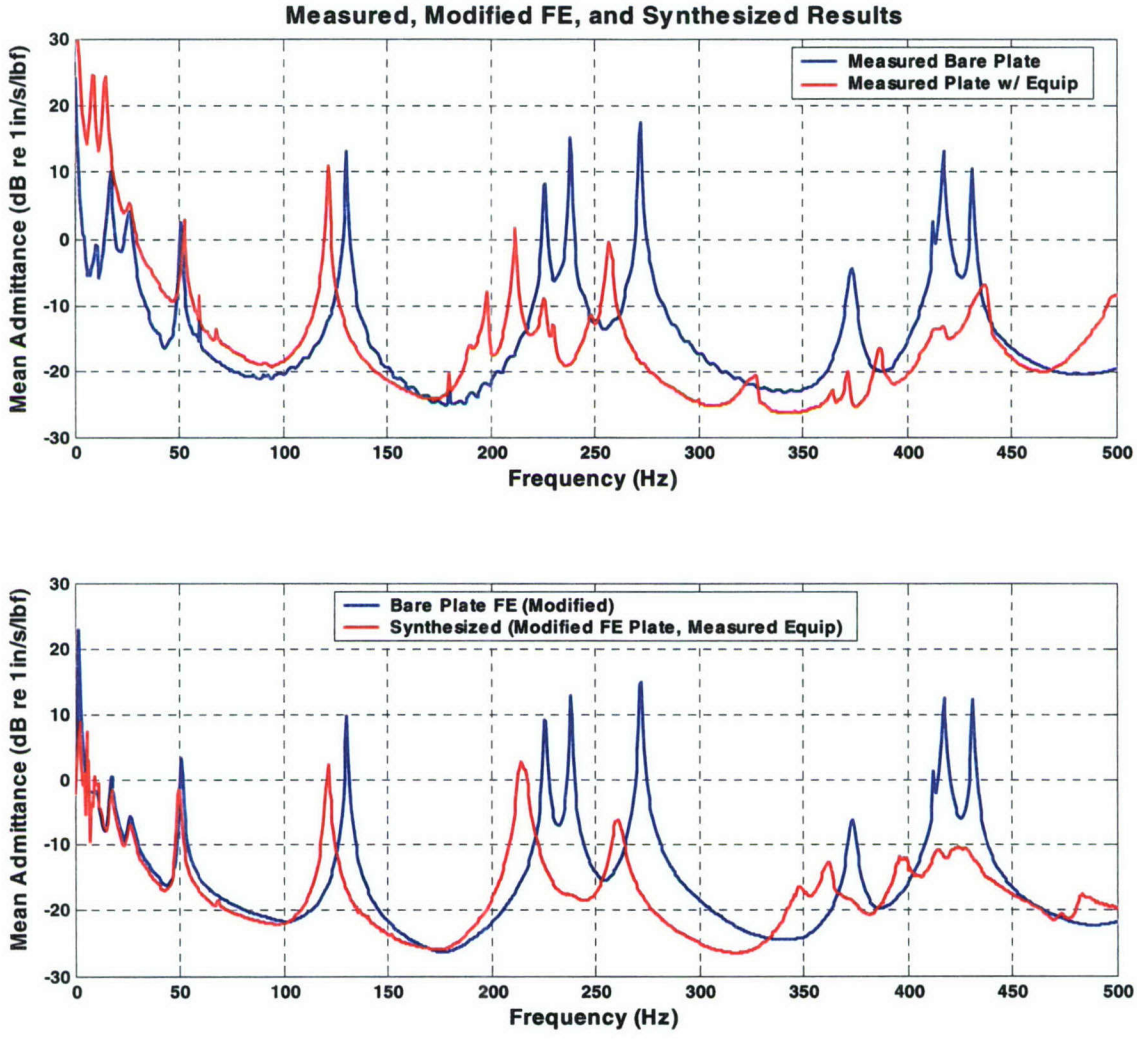

Figure 5.14. Measured and predicted bare plate and combined plate and equipment admittances

5.3.2 Thick Plate Treated with Waveguide Absorber Noise Control Elements

Folded beam waveguide absorbers (WGAs), shown in Figure 5.15, are damping devices which have been shown to provide broadband damping when attached to vibrating structures at points of high vibration amplitudes. The folded beam waveguide absorber is made by encasing a metal "folded beam" (encased everywhere except for the attachment face, see Figure 5.15b) in a viscoelastomer. The absorber is attached to the structure and the vibration energy is transmitted through the metal attachment face, into the absorber, and subsequently damped by the absorber's viscoelastic material.

Studies by Pray [14] and Munro [15] have shown that the damping contribution of the WGA is due to coupling of the translational and rotational degrees of freedom of the vibrating structure and absorber. Analytical formulations significantly underestimate the WGA damping contribution due to these coupling mechanisms. Munro's study showed that substructure

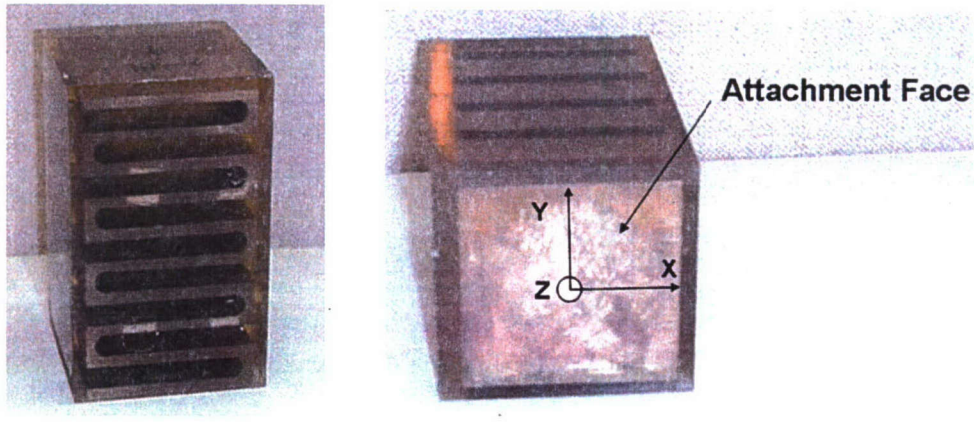

(a) (b)

Figure 5.15. Folded beam waveguide absorber (measures 2 in. square by $3^1/_8$ in. long) (a) side view and (b) bottom view

synthesis could be used to gain a much more accurate estimation of the WGA damping contribution. The objective of this example is to demonstrate the feasibility of FDSS for predicting coupled system loss factors, and also to demonstrate the importance of rotational degrees of freedom for the FDSS technique.

In this example, experimental mobilities of the WGA are coupled with numerical mobilities of a rectangular bronze alloy plate and the results are compared with experimental measurements of the WGA attached to the plate (the bronze alloy plate and an attached waveguide absorber are shown in Figure 5.16). The WGA is attached at several points along the length of the plate and the system loss factors are obtained for each attachment location. The purpose of translating the WGA along the plate length is to vary the amount of translation and rotation imparted to the WGA for any particular mode. The WGA is attached to the plate using a small metal spacer placed at the center of the attachment face. This condition is an approximation of a point attachment, which is simulated in the substructure synthesis computations via a single point attachment. The use of a single interface point in the FDSS computations necessitates the use of rotational degree of freedom information because the WGA rotational information is important for some of the plate modes. This importance is demonstrated by performing the FDSS both

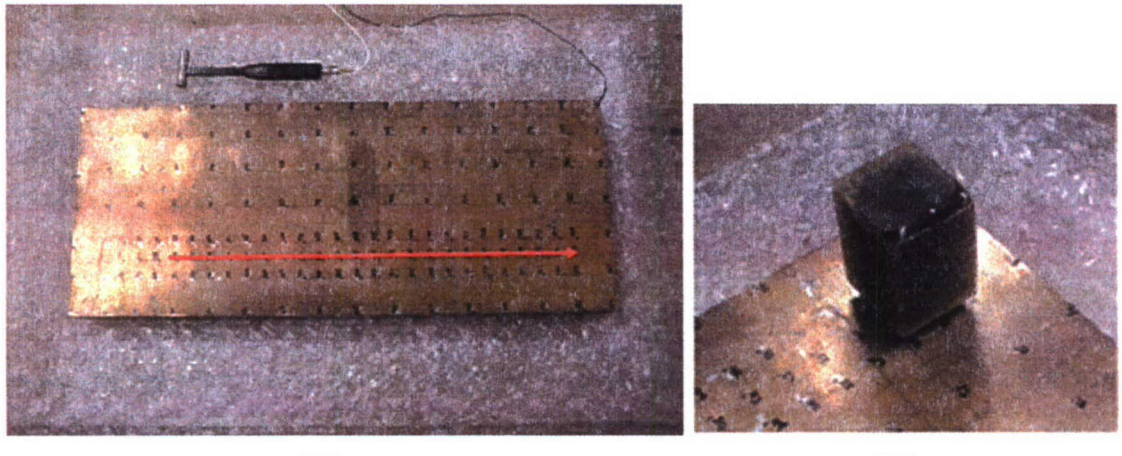

(a) (b)

Figure 5.16. (a) Bronze alloy plate (measuring 30 in. long, 12 in. wide, and 2 in. thick) with red arrow indicating WGA attachment region, and (b) WGA attached to plate with metal spacer

with and without the RDOF data and computing the coupled system loss factors for both cases. The rotational information is obtained using the finite difference approach described above in Section 4.3.

The plate is represented numerically using solid hexahedral finite elements (see Figure 5.17). The mobility matrices are generated using a modal summation solution with a modal basis set of 14 eigenvectors (6 of which are rigid body modes) obtained from MSC/Nastran 2004. Experimentally determined modal damping values are used in the modal summation solution.

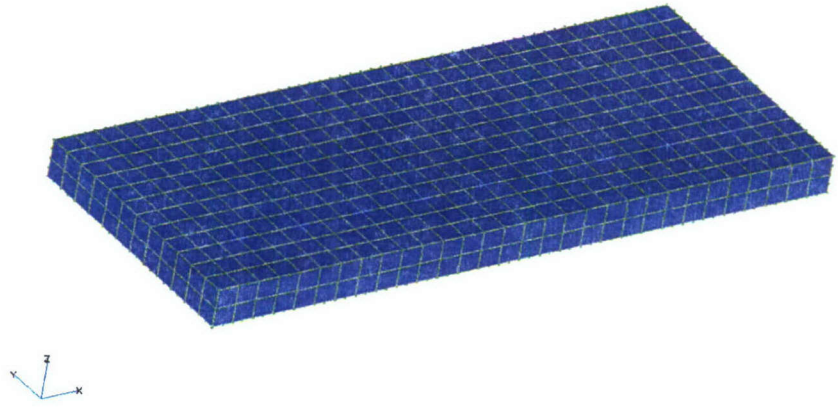

Figure 5.17. Bronze alloy plate finite element model constructed of quadratic hexahedral elements

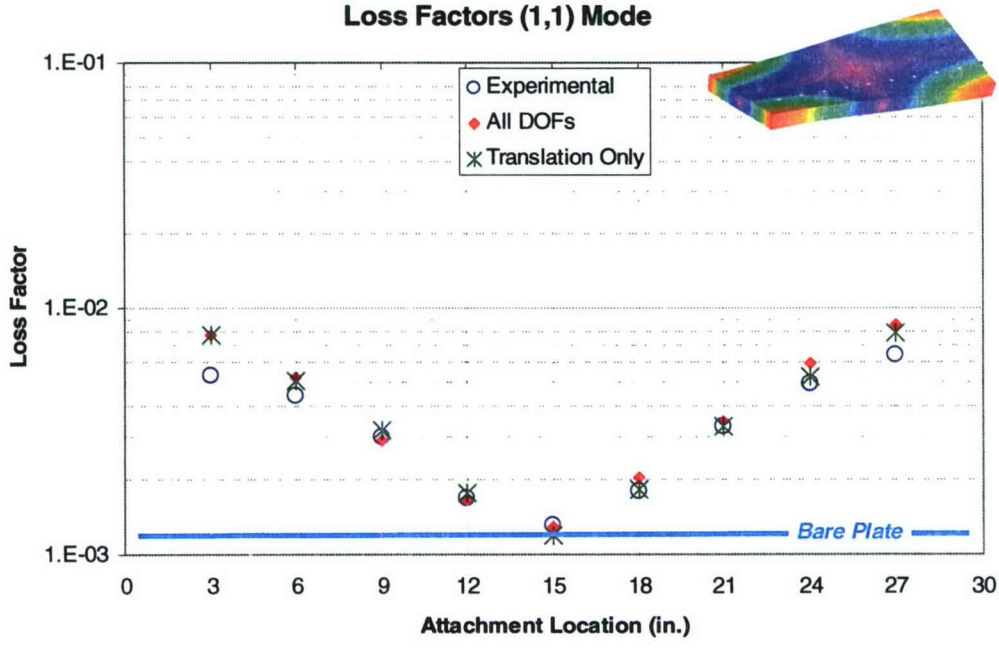

Figure 5.18. Measured and predicted system loss factors for the (1,1) mode (445 Hz) as the WGA is moved along the plate length

Damping comparisons between the measured and FDSS-predicted results for each of the nine attachment locations for the (1,1)[8] mode (resonance at 445 Hz) are shown in Figure 5.19. Two sets of predicted results are shown in this figure. The first set uses all six degrees of freedom at the attachment point, while the second set uses only the translational degrees of freedom. As indicated by these results, the measured and predicted damped plate loss factors agree well for all attachment locations. The predicted and measured damping level at the plate center is very similar to the undamped plate damping, which results from the lack of either rotational or translational motion at this location for the (1,1) mode. It can be concluded from these results that the rotational component of the mobility matrix does not play an important role at any of these nine attachment locations for the (1,1) mode.

Results for the (3,0) mode (resonance at 843 Hz)are shown in Figure 5.19. As indicated by these results, the measured and predicted damped plate loss factors agree well for all locations except at the plate center. When the WGA is attached at the plate center for this mode, the WGA sees only a rotational component of plate motion and thus the translational-only FDSS shows no effect of the WGA and the coupled system loss factor is identical to the bare plate loss factor. Two of the attachment locations, 9 in. and 21 in., experience pure translation and thus the predicted loss factors for both FDSS solutions are identical at these locations.

Based on these results it can be concluded that mobilites involving the rotational DOFs can be an important component of the FDSS technique. As discussed in Section 4.3 the use of rotational degrees of freedom are generally important when the attachment interface cannot support rotation though a broad placement of the translation DOFs. This example employed coupling at

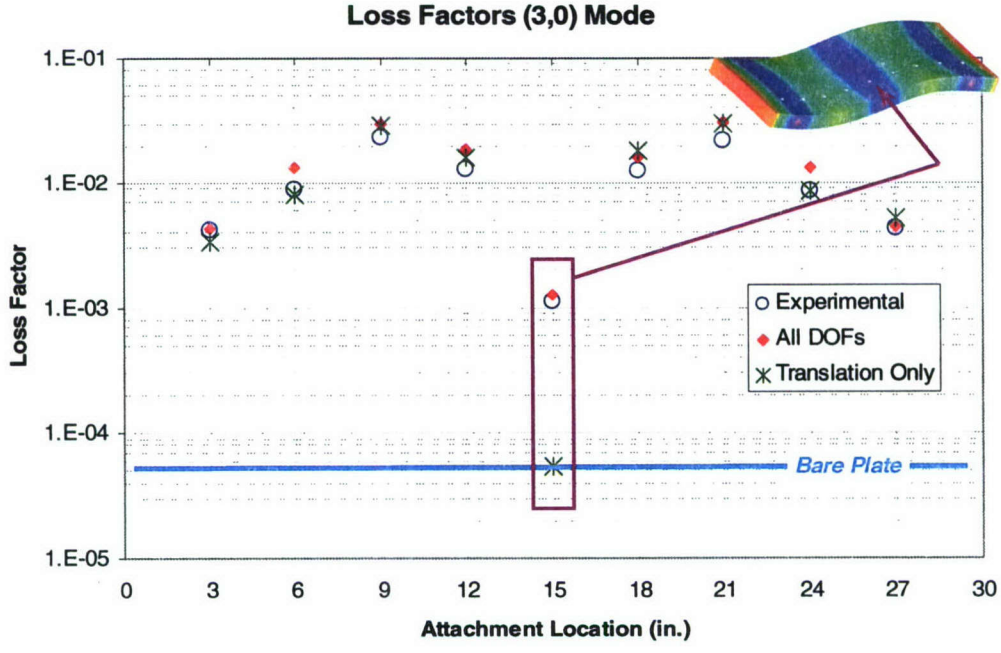

Figure 5.19. Measured and predicted system loss factors for the (3,0) mode (843 Hz) as the WGA is moved along the plate length

[8] Mode classification for a free-free plate is (number of nodal lines along length, number of nodal lines along width).

a single location and thus the RDOFs can play an important role as is demonstrated for the (3,0) mode.

6 Summary and Conclusions

An overview of impedance- and modal-based substructure analysis techniques is presented. While both techniques are applicable to data sets of varying origin (i.e., numerical and experimental), the impedance technique is generally preferred because of the difficulty often involved in accurately determining mode shapes from an experimental data set. Of particular interest herein is the combination of numerically and experimentally derived frequency response data, which is especially useful for a structural model comprised of components that are too complex to represent with the finite element technique. The present work focuses on the frequency domain substructure synthesis algorithm introduced by Jetmundsen *et al* [1] since this algorithm offers a significant improvement over the traditional frequency domain technique in terms of the processing requirements. The method is also amenable to interfacial impedances and offers completely arbitrary interface definitions for the multiple substructures. The interfaces are defined via a Boolean mapping matrix that uses an arbitrary interface sign convention.

The practical limitations of the frequency domain techniques are identified as modal truncation and incomplete mobility matrices. The modal truncation effects are only relevant for modal summation solutions, but can be corrected through the inclusion of residual terms. Incomplete mobility matrices are a result of the current technological limitations for measuring rotational mobilities at a point. However, techniques have been developed to estimate these components.

The modal coupling techniques offer a method to incorporate general frequency-dependent coupling matrices into a modal frequency response solution. This technique also allows large finite element models to be separated into smaller models that are solved individually and then combined through their eigenvectors and impedance coupling matrices. Eigenvectors for the coupled system can be obtained using singular value decomposition or an eigenanalysis, which operate on the coupled system equation in modal coordinates. The practical limitations of the modal coupling techniques is identified as modal truncation.

Example problems were presented to demonstrate the capabilities and limitations of the techniques described herein. The example regarding modal substructuring showed resonance frequency predictions with error on the order of 0.5% and indicated potential improvements by an expanded basis set. Frequency domain substructure synthesis examples demonstrated the usefulness of the technique to predict resonance frequencies and damping for the coupled system and also showed the importance of rotational degrees of freedom to the accuracy of the coupling.

7 References

1. Jetmundsen, B., Bielawa, R. L., Flannelly, W. G., "Generalized Frequency Domain Substructure Synthesis," *Journal of the American Helicopter Society*, 1988, pp. 55-64.
2. ABAQUS/Standard User's Manual, Volume 1, Version 5.6, 1996.
3. Avitabile, P., "Twenty Years of Structural Dynamic Modification – A Review," *Journal of Sound and Vibration*, **37**(1), 2003, pp. 14-27.

4. D'Ambrogio, W., Sestieri, A., "Substructure Coupling Using FRFS: Strategies for Tackling Rotational Degrees of Freedom," International Conference on Structural Dynamics Modeling, Portugal, 3-5 June, 2002.

5. Ewins, D. J., Modal Testing: Theory and Practice. John Wiley & Sons Incorporated, New York, NY, 1995.

6. Fahnline, J. B., "Computing Fluid-Coupled Resonance Frequencies, Mode Shapes, and Damping Loss Factors Using the Singular Value Decomposition," *Journal of Acoustical Society of America*, **115**(4), 2004, pp. 1-9.

7. Giordano, J. A., Koopmann, G. H., "State space boundary element–finite element for fluid-structure interaction analysis," *Journal of Acoustical Society of America*, **98**, 1995, pp. 363-372.

8. Cunefare, K. A., De Rosa, S., "An improved state-space method for coupled fluid-structure interaction analysis," *Journal of Acoustical Society of America*, **105**, 1999, pp. 206-210.

9. Gordis, J. H., Bielawa, R. L., and Flannelly, W. G., "A General Theory for Frequency Domain Structural Synthesis," *Journal of Sound and Vibration*, **150**(1), 1991, pp. 139-158.

10. Duarte, M. M., Ewins, D. J., "Rotational Degrees of Freedom for Structural Coupling Analysis via Finite-Difference Technique with Residual Compensation," *Mechanical Systems and Signal Processing*, **14**(2), 2000, pp. 205-227.

11. ANSI S2.34-1984, "American National Standard: Guide to the Experimental Determination of Rotational Mobility Properties and the Complete Mobility Matrix." Acoustical Society of America, New York.

12. McDevitt, T. E., Campbell, R. L., Jenkins, D. M., Jonson, M. L., and Hambric, S. A., "Structural-Acoustic Issues Associated with Modeling Motor Noise Mechanisms," The Pennsylvania State University Applied Research Laboratory Technical Memorandum 03-010, March 2003.

13. Campbell, R. L., and Hambric, S. A., "Effects of Equipment Loading on The Vibrations of Edge-Stiffened Plates and Associated Modeling Issues," *Proceedings of 2002 ASME International Mechanical Engineering Congress and Exposition*, November 17-22, 2002, New Orleans, LA.

14. Pray, C. M., Hambric, S. A., and McDevitt, T. E. "Folded Beam Waveguide Absorbers," *Noise Control Engineering Journal*, November, 2001.

15. Munro, A. D., "Loss Factor Prediction For Folded Beam Waveguide Absorbers Using Translational and Rotational Degree of Freedom Frequency Response Function Coupling." Master's Thesis, The Pennsylvania State University, 2002.